Quark Matter under Extreme Conditions
极端条件下的夸克物质

张辉　(Hui Zhang)

Institute of Quantum Matter, South China Normal University, Guangzhou

Jul. 9th, 2022, IQM, SCNU

Signatures of Chiral Magnetic Effect in the Collisions of Isobars, Shuzhe Shi, **HZ**, Defu Hou, Jinfeng Liao, Phys. Rev. Lett. 125, 242301 (2020)
Mesonic Condensation in Isospin Matter under Rotation, **HZ**, Defu Hou, Jinfeng Liao, Chin.Phys.C 44 (2020) 11, 111001
Hyperon polarization from the vortical fluid in low-energy nuclear collisions, Yu Guo, Jinfeng Liao, Enke Wang, Hongxi Xing, **HZ**, Phys.Rev.C 104 (2021) 4, L041902

Introduction

Quark Matter in Strong Magnetic Field

Quark Matter under Rotation

Vorticity in HIC

Structure of Matter: An Ancient Quest

Empedocles:
four elements ---
fire, air, water, earth

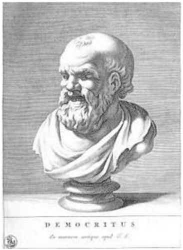

Democritus:
atomic hypothesis

Laozi

道生一
一生二
二生三
三生万物

All matter is made from a set of fundamental entities

The physical world has a hierarchy of structures.

matter

molecule

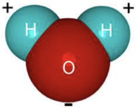

atoms

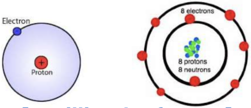

[a millionth of a mm]

atomic nucleus

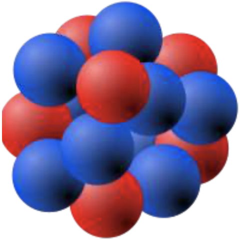

[a trillionth of a mm]

proton

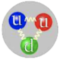

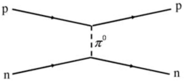

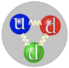

neutron

nuclear force

Most basic entities: quarks and gluons.

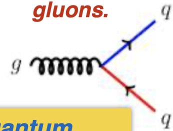

Quantum Chromodynamics (QCD)

Standard Model of Elementary Particles

粒子物理标准模型

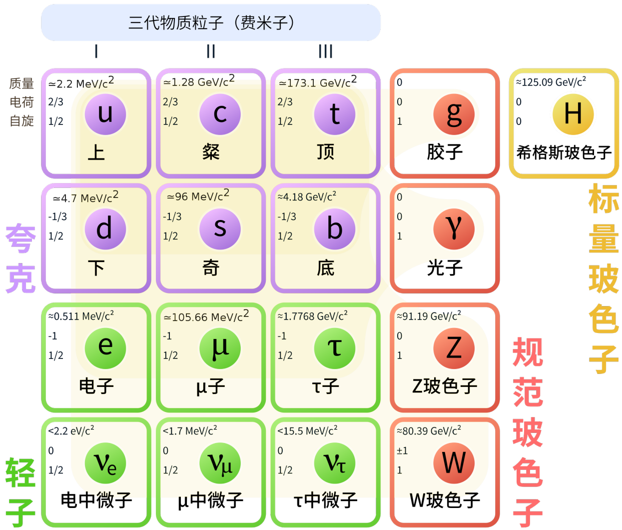

Quantum Chromodynamics (QCD)

The fundamental theory of strong nuclear force: QCD, a non-Abelian gauge theory of quarks and gluons

$$\mathcal{L} = \bar{\psi}(i\partial\!\!\!/ - M - g A\!\!\!/_a G^a)\psi - \frac{1}{4} F_a^{\mu\nu} F^a_{\mu\nu}$$

$$F_a^{\mu\nu} = \partial^\mu A_a^\nu - \partial^\nu A_a^\mu - g f_{abc} A_b^\mu A_c^\nu$$

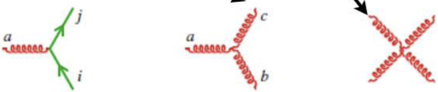

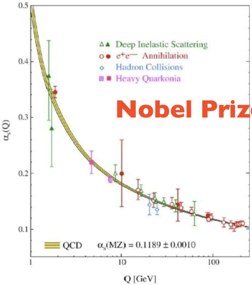

Nobel Prize 2004

Asymptotic Freedom: coupling becomes large at low energy or long distance scale.

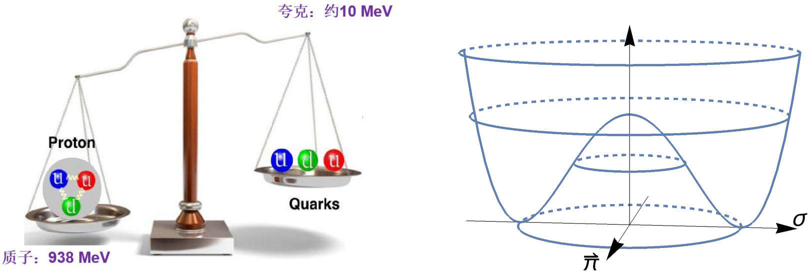

Figure: Spontaneously broken chiral symmetry in the vacuum is a fundamental property of QCD

Phase Diagram of Water

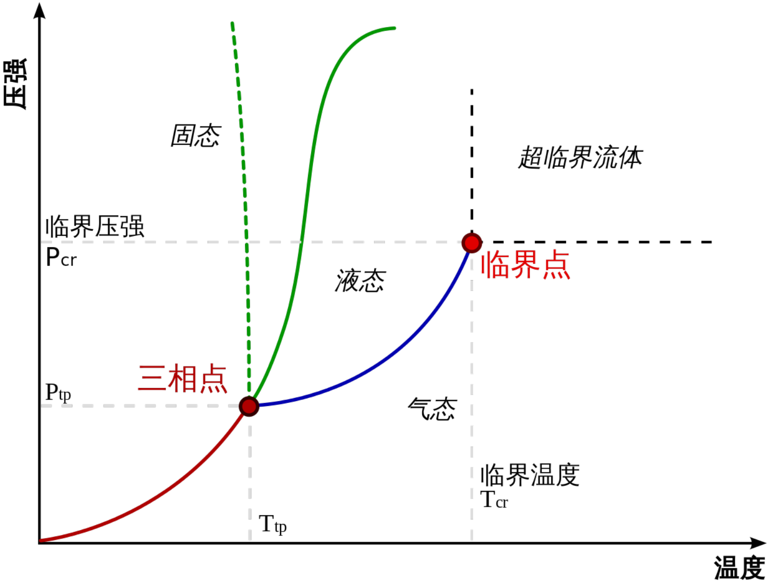

QCD Phase Diagram

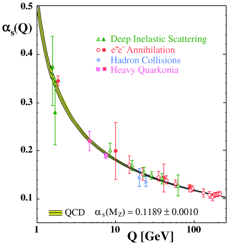

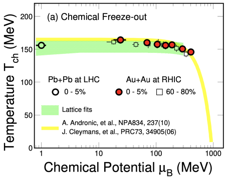

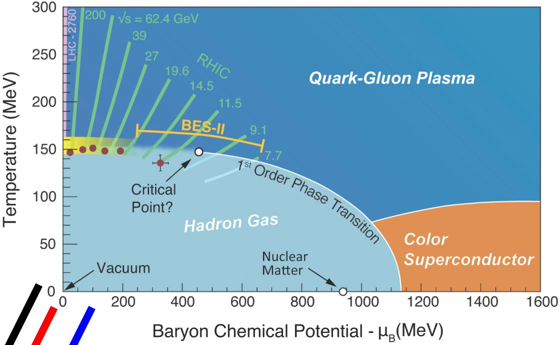

$\vec{B}$ $\vec{\omega}$ "C"

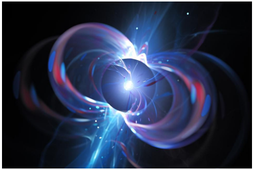

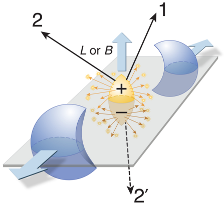

Opening up new dimensions:
Toward Hyper-Phase-Diagram!

Heavy Ion Collision

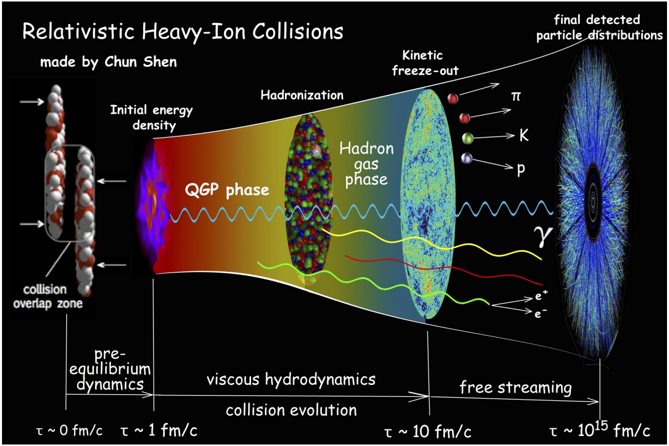

Quark-gluon plasma is created in such collisions!

The hottest matter!

The most perfect fluid!

Heavy Ion Collision

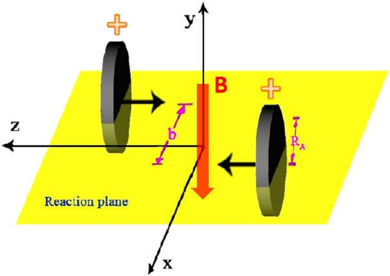

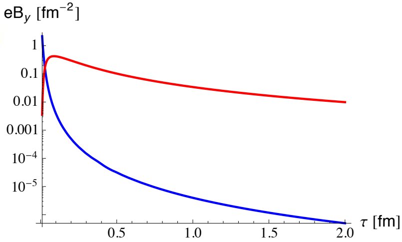

Strongest EM fields

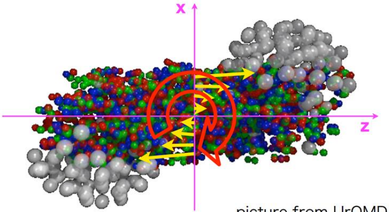

picture from UrQMD

Largest local rotation

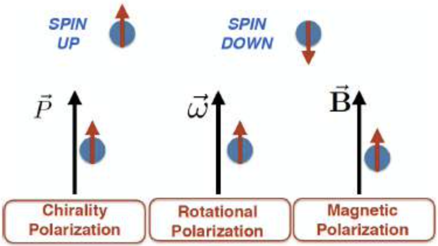

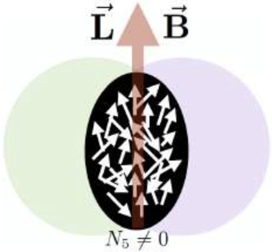

[arXiv:2004.00569]

The interplay of spin with chirality/vorticity/magnetic field ⇒ many novel phenomena

Dirac fermion in rotation & B field

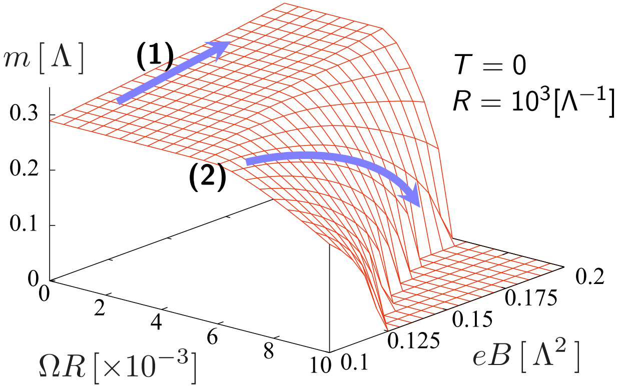

Rotational magnetic inhibition

(1) eB increases $\longrightarrow$ M increases: **Magnetic Catalysis**

(2) eB increases $\longrightarrow$ M decreases: **Inverse of MC**

Chen, Fukushima, Huang & Mameda, PRD2016

Chiral Magnetic Effect

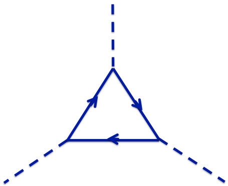

Figure: The triangle diagram involving the charged chiral fermion loop, a composite axial or dilatational current, and two external gauge fields.
Prog.Part.Nucl.Phys. 75 (2014) 133-151

$$\vec{J} = \frac{e^2}{2\pi^2}\mu_5\vec{B}$$

Chiral Magnetic Effect

AVFD: Anomalous-Viscous Fluid Dynamics

$$\hat{D}_\mu J_R^\mu = +\frac{N_c Q^2}{4\pi^2} E_\mu B^\mu, \qquad \hat{D}_\mu J_L^\mu = -\frac{N_c Q^2}{4\pi^2} E_\mu B^\mu$$

CME

$$J_R^\mu = n_R\, u^\mu + \boxed{\nu_R^\mu} + \boxed{\frac{N_c Q}{4\pi^2} \mu_R B^\mu}$$

$$J_L^\mu = n_L\, u^\mu + \boxed{\nu_L^\mu} - \boxed{\frac{N_c Q}{4\pi^2} \mu_L B^\mu}$$

Viscous Effect

$$\Delta_\nu^\mu \hat{d}\left(\nu_\chi^\nu\right) = -\frac{1}{\tau_r}\left[\left(\nu_\chi^\mu\right) - \left(\nu_\chi^\mu\right)_{NS}\right]$$

$$\left(\nu_\chi^\mu\right)_{NS} = \frac{\sigma}{2} T \Delta^{\mu\nu} \partial_\nu \left(\frac{\mu_{\chi,f}}{T}\right) + \frac{\sigma}{2} Q E^\mu$$

AVFD

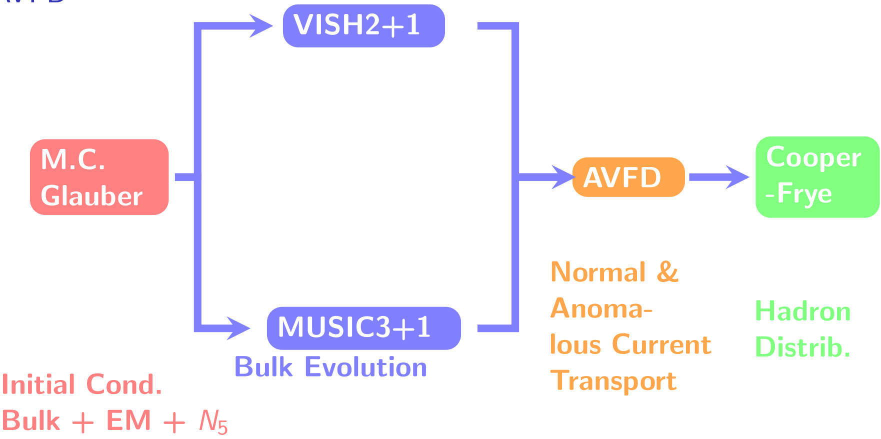
VISH2+1
M.C. Glauber
AVFD
Cooper -Frye
MUSIC3+1
Bulk Evolution
Initial Cond.
Bulk + EM + N_5
Normal & Anoma- lous Current Transport
Hadron Distrib.

Chiral Magnetic Effect

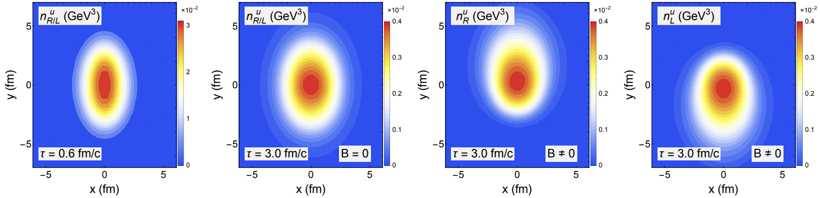

$$E\frac{d^3N}{dp^3} = \frac{d^3N}{p_T dp_T dy d\phi} = \frac{d^2N}{p_T dp_T dy}\frac{1}{2\pi} \times$$

$$\left[1 + 2\sum_{n=1}^{\infty} a_n(p_t, y)\sin\left(n\left(\phi - \Psi_n\right)\right) + 2\sum_{n=1}^{\infty} v_n(p_t, y)\cos\left(n\left(\phi - \Psi_n\right)\right)\right]$$

$$\gamma = \langle cos\Delta\phi_i cos\Delta\phi_j\rangle - \langle sin\Delta\phi_i sin\Delta\phi_j\rangle = \kappa v_2 F - H$$

$$\delta = \langle cos\Delta\phi_i cos\Delta\phi_j\rangle + \langle sin\Delta\phi_i sin\Delta\phi_j\rangle = F + H$$

F: Bulk Background H: Possible CME Signal

Isobaric Collisions: $^{96}_{44}Ru^{96}_{44}Ru$ vs. $^{96}_{40}Zr^{96}_{40}Zr$

New opportunity of potential discovery: Isobaric Collision @ RHIC

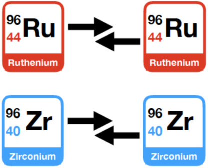

Key idea: contrasting two systems with identical bulk, varied magnetic fields.

Koch, et al, arXiv: 1608.00982

Charge Asymmetry Correlation Measurement

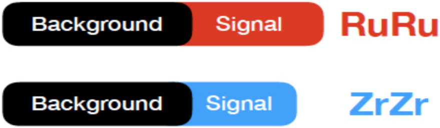

Event Selection for the Isobaric Collisions: Insights from Initial Conditions

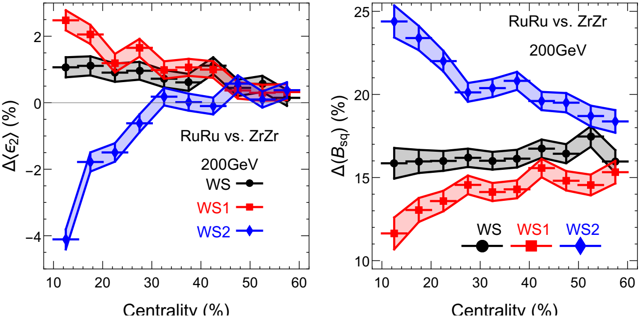

Figure: The relative difference in eccentricity $\Delta\langle\epsilon_2\rangle$ (left) and projected magnetic-field-strength-squared $\Delta(B_{sq})$ (right) between RuRu and ZrZr, with conventional centrality event selection.

Event Selection for the Isobaric Collisions: Insights from Initial Conditions

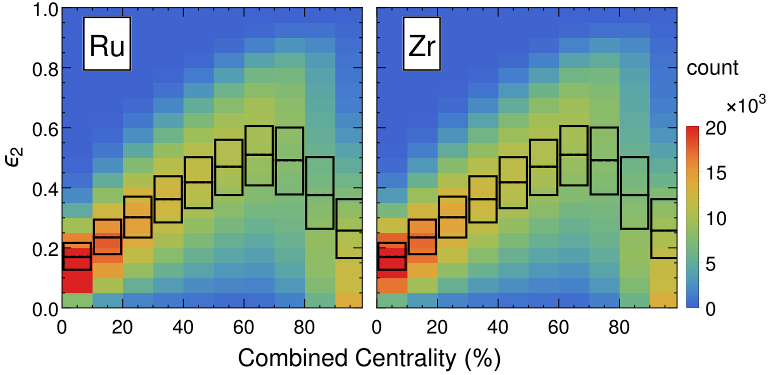

Figure: joint (multiplicity + elliptic-flow) identical event selection

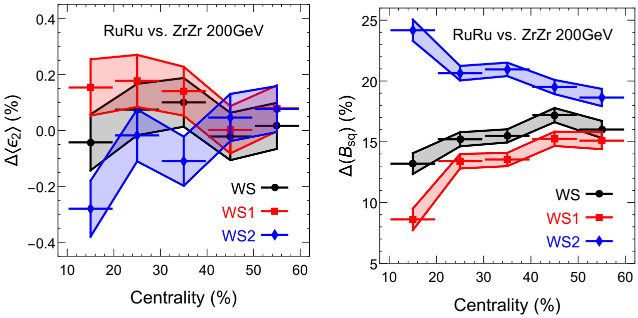

Figure: The relative difference in eccentricity $\Delta\langle\epsilon_2\rangle$ (left) and projected magnetic-field-strength-squared $\Delta(B_{sq})$ (right) between RuRu and ZrZr, with the proposed joint (multiplicity + elliptic-flow) event selection.

Isobaric Collisions: $^{96}_{44}Ru^{96}_{44}Ru$ vs. $^{96}_{40}Zr^{96}_{40}Zr$

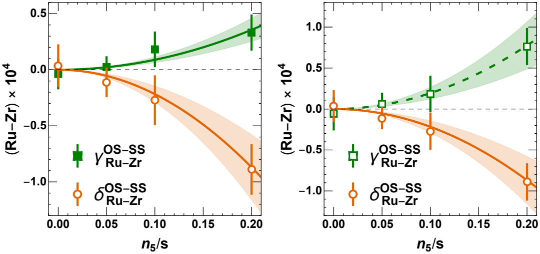

Figure: The absolute difference in correlation observables $(\gamma^{OS-SS}_{Ru} - \gamma^{OS-SS}_{Zr})$ and $(\delta^{OS-SS}_{Ru} - \delta^{OS-SS}_{Zr})$ with respect to event-plane (EP: left panel) and reaction plane (RP: right panel) geometry, measured with post-selection events, for varied signal strength as controlled by initial axial charge density n_5/s.

$$\xi^{EP}_{isobar} \equiv \frac{\gamma^{OS-SS}_{Ru-Zr}|_{EP}}{\delta^{OS-SS}_{Ru-Zr}|_{EP}} \simeq -(0.41 \pm 0.27)$$

$$\xi^{RP}_{isobar} \equiv \frac{\gamma^{OS-SS}_{Ru-Zr}|_{RP}}{\delta^{OS-SS}_{Ru-Zr}|_{RP}} \simeq -(0.90 \pm 0.45)$$

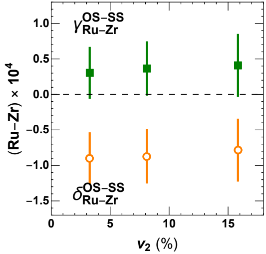

Figure: Predictions from EBE-AVFD simulations for observables $(\gamma^{OS-SS}_{Ru} - \gamma^{OS-SS}_{Zr})$ and $(\delta^{OS-SS}_{Ru} - \delta^{OS-SS}_{Zr})$ as a function of bin-wise elliptic flow v_2 from event-shape analysis with three identical bins for RuRu and ZrZr systems. The simulation results are obtained with $n_5/s = 20\%$.

However

PHYSICAL REVIEW C **105**, 014901 (2022)

Search for the chiral magnetic effect with isobar collisions at $\sqrt{s_{NN}} = 200$ GeV by the STAR Collaboration at the BNL Relativistic Heavy Ion Collider

(Received 31 August 2021; accepted 7 December 2021; published 3 January 2022)

The chiral magnetic effect (CME) is predicted to occur as a consequence of a local violation of $\mathcal{P}$ and $\mathcal{CP}$ symmetries of the strong interaction amidst a strong electromagnetic field generated in relativistic heavy-ion collisions. Experimental manifestation of the CME involves a separation of positively and negatively charged hadrons along the direction of the magnetic field. Previous measurements of the CME-sensitive charge-separation observables remain inconclusive because of large background contributions. To better control the influence of signal and backgrounds, the STAR Collaboration performed a blind analysis of a large data sample of approximately 3.8 billion isobar collisions of ${}^{96}_{44}\mathrm{Ru} + {}^{96}_{44}\mathrm{Ru}$ and ${}^{96}_{40}\mathrm{Zr} + {}^{96}_{40}\mathrm{Zr}$ at $\sqrt{s_{NN}} = 200$ GeV. Prior to the blind analysis, the CME signatures are predefined as a significant excess of the CME-sensitive observables in Ru + Ru collisions over those in Zr + Zr collisions, owing to a larger magnetic field in the former. A precision down to 0.4% is achieved, as anticipated, in the relative magnitudes of the pertinent observables between the two isobar systems. Observed differences in the multiplicity and flow harmonics at the matching centrality indicate that the magnitude of the CME background is different between the two species. No CME signature that satisfies the predefined criteria has been observed in isobar collisions in this blind analysis.

DOI: 10.1103/PhysRevC.105.014901

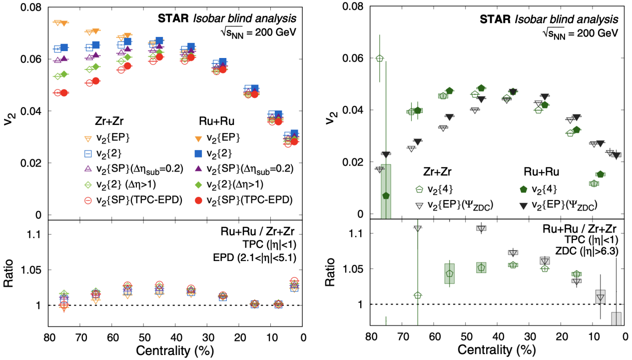

FIG. 4. (Left) Elliptic anisotropy v_2 measurements using different methods in isobar collisions at $\sqrt{s_{NN}} = 200$ GeV as a function of centrality using TPC and EPD detectors. In the upper panels, the solid and open symbols represent measurements for Ru + Ru and Zr + Zr collisions, respectively. The data points are shifted along the x axis for clarity. The lower panels show the v_2 ratios in Ru + Ru over Zr + Zr collisions. The statistical uncertainties are represented by lines and systematic uncertainties by boxes. (Right) The same showing measurements for four particle correlations using TPC and EP determined from ZDC. The data points are shifted horizontally for clarity.

However

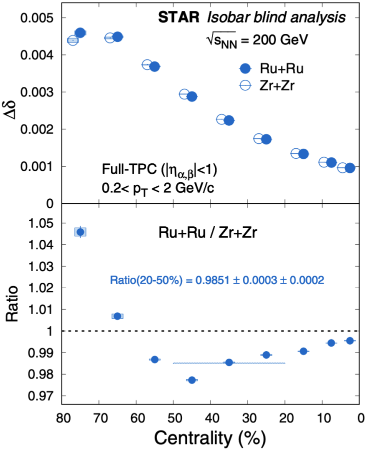

FIG. 7. $\Delta\delta$ measured for Ru + Ru and Zr + Zr collisions at $\sqrt{s_{NN}}$ = 200 GeV (upper panel) and the ratio of Ru + Ru to Zr + Zr (lower panel). The centrality bins are shifted horizontally for clarity. The border-less horizontal bands denote the statistical uncertainties. The horizontal bands with the dashed border represent the systematic uncertainties.

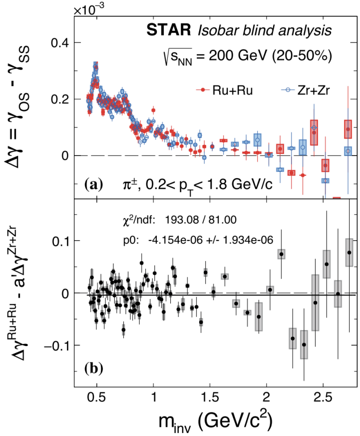

FIG. 17. The $\Delta\gamma$ in 20–50% Ru + Ru and Zr + Zr collisions (a) and their difference defined by Eq. (24) (b) as functions of the $\pi^+\pi^-$ invariant mass m_{inv}. The difference in the lower panel would measure the possible CME if the background in $\Delta\gamma$ scales with v_2 only [$a' = v_2^{\mathrm{Ru+Ru}}/v_2^{\mathrm{Zr+Zr}}$ as defined by Eq. (25)]. Error bars are statistical and shaded boxes are systematic uncertainties. The solid line in the lower panel is a constant fit to the data.

However

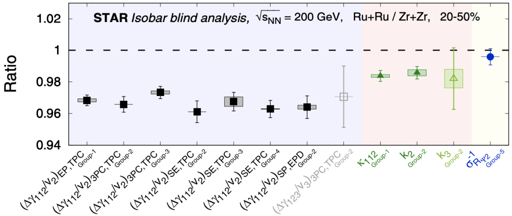

FIG. 26. Compilation of results from the blind analysis. Only results contrasting between the two isobar systems are shown. Results are shown in terms of the ratio of measures in Ru + Ru collisions over Zr + Zr collisions. Solid dark symbols show CME-sensitive measures whereas open light symbols show counterpart measures that are supposed to be insensitive to CME. The vertical lines indicate statistical uncertainties whereas boxes indicate systematic uncertainties. The colors in the background are intended to separate different types of measures. The fact that CME-sensitive observable ratios lie below unity leads to the conclusion that no predefined CME signatures are observed in this blind analysis.

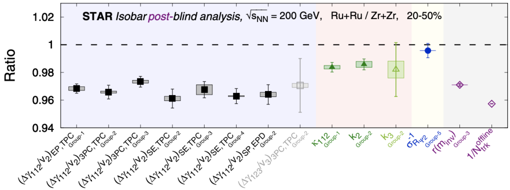

FIG. 27. Compilation of post-blinding results. This figure is largely the same as Fig. 26 with the following differences: numerical changes in the results from the new run-by-run QA algorithm are treated as an additional systematic uncertainty added in quadrature, and two data points (open markers) have been added on the right to indicate the ratio of inverse multiplicities ($N_{\mathrm{trk}}^{\mathrm{offline}}$) and the ratio of relative pair multiplicity difference (r) as explained in the text.

QCD with large angular momentum: HIC

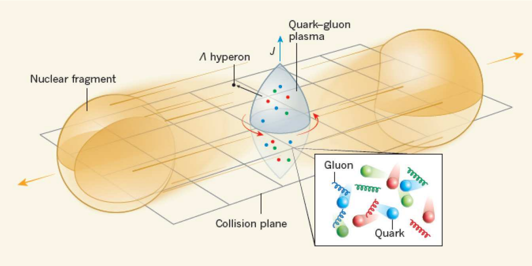

Figure: Off-central HIC

Rotational polarization effect → Anomalous effects: Chiral vortical effect, Chiral vortical wave...

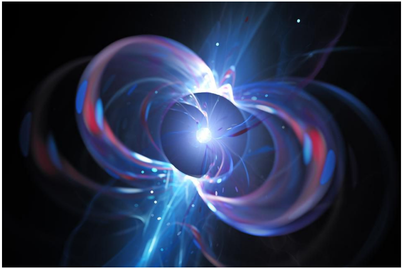

Figure: Spin Neutron Star.

Rotational Supression of fermion pairing in J=0 (PRL 117, no.19(2016)192302) This study (first): isospin matter
Isospin chemical potential: imbalance between the u-flavor and d-flavor of quarks

Phase Diagram of QCD for $n_u \neq n_d$

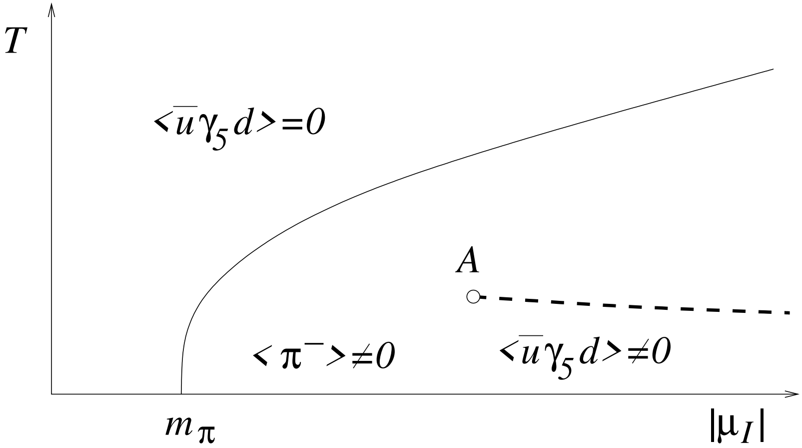

Figure: D. T. Son and M. A. Stephanov, Phys. Rev. Lett. 86, 592 (2001)

Dirac fermion in rotation & B field

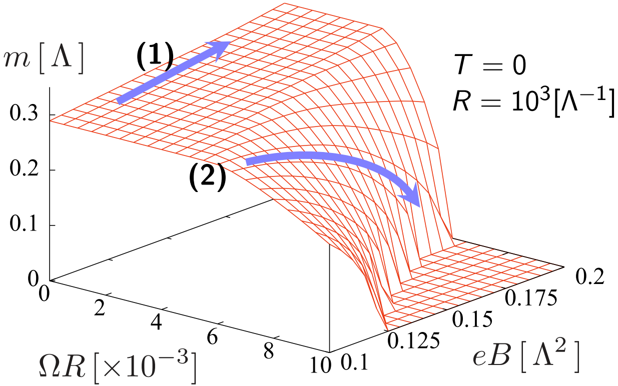

Rotational magnetic inhibition

(1) eB increases $\longrightarrow$ M increases: **Magnetic Catalysis**

(2) eB increases $\longrightarrow$ M decreases: **Inverse of MC**

Chen, Fukushima, Huang & Mameda, PRD2016

Rotation suppression of scalar pairing

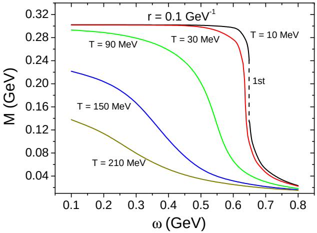

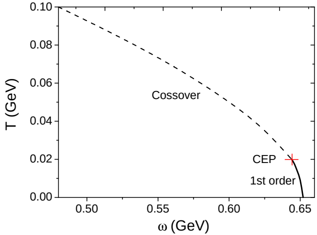

Jiang & Liao PRL2016

Description of rotating system

Dirac Lagrangian in rotating frame

$$g_{\mu\nu} = \begin{pmatrix} 1-\vec{v}^2 & -v_1 & -v_2 & -v_3 \\ -v_1 & -1 & 0 & 0 \\ -v_2 & 0 & -1 & 0 \\ -v_3 & 0 & 0 & -1 \end{pmatrix} \begin{matrix} \bar{\gamma}^\mu = e_a{}^\mu \gamma^a \\ \Gamma_\mu = \frac{1}{4}\cdot\frac{1}{2}[\gamma^a,\gamma^b]\,\Gamma_{ab\mu} \end{matrix}$$

$$\vec{v} = \vec{\omega}\times\vec{x} \quad \Longrightarrow \quad \mathcal{L} = \bar{\psi}\,[i\bar{\gamma}^\mu(\partial_\mu + \Gamma_\mu) - m]\,\psi$$

Under slow rotation:

$$\begin{aligned} \mathcal{L} &= \psi^\dagger \left[i\partial_0 + i\gamma^0\vec{\gamma}\cdot\vec{\partial} + (\vec{\omega}\times\vec{x})\cdot(-i\vec{\partial}) + \vec{\omega}\cdot\vec{S}_{4\times 4} \right]\psi \\ \hat{H} &= \gamma^0(\vec{\gamma}\cdot\vec{p} + m) - \vec{\omega}\cdot(\vec{x}\times\vec{p} + \vec{S}_{4\times 4}) \\ &= \hat{H}_0 - \boxed{\vec{\omega}\cdot\hat{\vec{J}}} \;\; \textit{rotational polarization effect!} \end{aligned}$$

$$\sigma = \langle\bar{\psi}\psi\rangle,\;\; \pi = \langle\bar{\psi}i\gamma_5\boldsymbol{\tau}\psi\rangle,\;\; \rho = \langle\bar{\psi}i\gamma_0\tau_3\psi\rangle$$

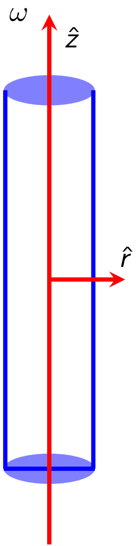

Model

$$\mathcal{L} = \bar{\psi}(i\gamma_\mu\partial^\mu - m_0 + \frac{\mu_I}{2}\gamma_0\tau_3)\psi \quad + \quad G_s\left[\left(\bar{\psi}\psi\right)^2 + \left(\bar{\psi}i\gamma_5\boldsymbol{\tau}\psi\right)^2\right] \quad - \quad G_v\left(\bar{\psi}\gamma_\mu\boldsymbol{\tau}\psi\right)^2$$

$$\mathcal{L}_R = \psi^\dagger\left[(\vec{\omega}\times\vec{x})\cdot(-i\vec{\partial}) + \vec{\omega}\cdot\vec{S}_{4\times 4}\right]\psi$$

MF approximation:

$$\sigma = \langle\bar{\psi}\psi\rangle,\ \pi = \langle\bar{\psi}i\gamma_5\boldsymbol{\tau}\psi\rangle,\ \rho = \langle\bar{\psi}i\gamma_0\tau_3\psi\rangle$$

Model

$$\Omega = G_s(\sigma^2 + \pi^2) - G_v\rho^2$$
$$-\frac{\mathrm{N_c N_f}}{16\pi^2}\sum_n \int \mathrm{d}k_t^2 \int \mathrm{d}k_z [J_{n+1}(k_t r)^2 + J_n(k_t r)^2] T \times$$
$$\Big[\ln\Big(1+\exp(-\frac{\omega^+ - (n+\frac{1}{2})\omega}{T})\Big) + \ln\Big(1+\exp(\frac{\omega^+ - (n+\frac{1}{2})\omega}{T})\Big)$$
$$+\ln\Big(1+\exp(-\frac{\omega^- - (n+\frac{1}{2})\omega}{T})\Big) + \ln\Big(1+\exp(\frac{\omega^- - (n+\frac{1}{2})\omega}{T})\Big)\Big]$$

$$\omega^\pm = \sqrt{4G_s^2\pi^2 + (\sqrt{(m_0 - 2G_s\sigma)^2 + k_t^2 + k_z^2} \pm \widetilde{\mu}_I)^2}, \quad \widetilde{\mu}_I = \frac{\mu_I}{2} + G_v\,\rho$$

Gap equation: $\frac{\partial\Omega}{\partial\sigma} = \frac{\partial\Omega}{\partial\pi} = \frac{\partial\Omega}{\partial\rho} = 0$

σ, π Channel

Rotational Suppression on Pion Superfluidity

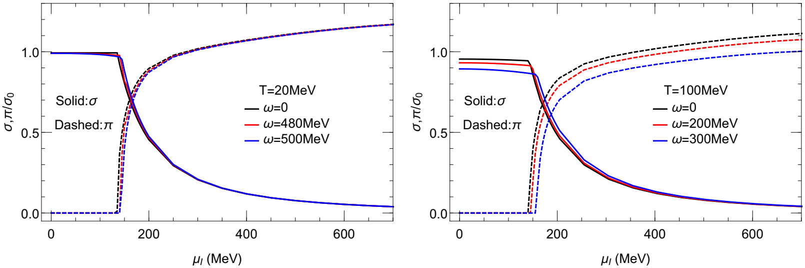

Figure: Suppression effect is consistent with (PRL117, no.19 (2016) 192302). inverse catalysis effect

$\sigma : s = 1, L = 1, J = 0;$ $\qquad\qquad$ $\pi : s = 0, L = 0, J = 0$

Rotation weaken spin 0 condensate: inverse catalysis effect

Rotational Suppression on Pion Superfluidity

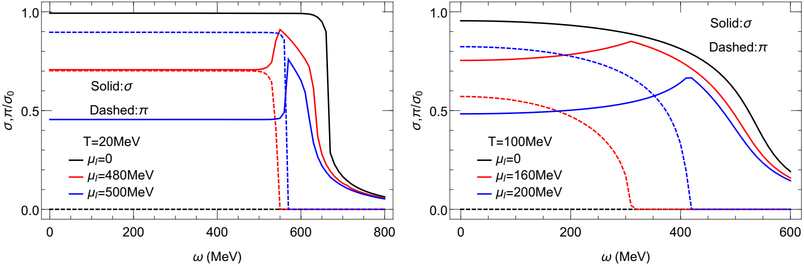

Figure: Prefer σ than π

$\sigma : s = 1, L = 1, J = 0;$ $\quad\quad$ $\pi : s = 0, L = 0, J = 0$

Rotation weaken spin 0 condensate: inverse catalysis effect

Pion superfluidity phase diagram in $T - \mu_I$

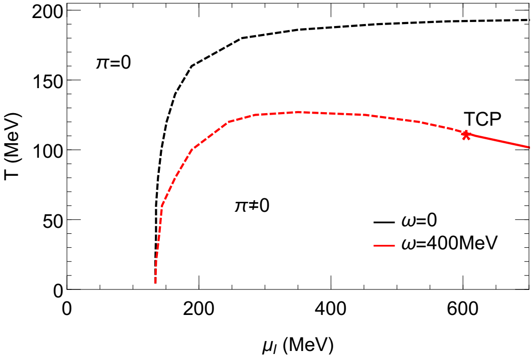

Figure: Dashed line stands for the second-order phase transition, while solid for the first-order. The star denotes a tri-critical point (TCP).

Enhanced ρ Superfluidity under Rotation

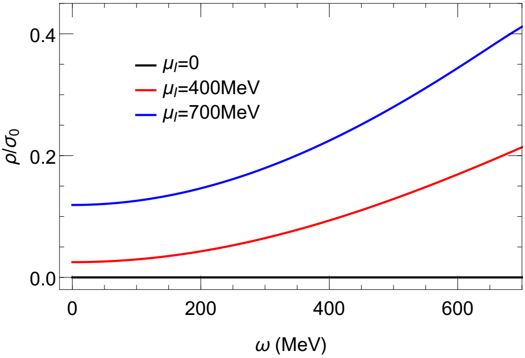

Figure: Rotation weaken spin 0 condensate, but enhance spin 1 condensate

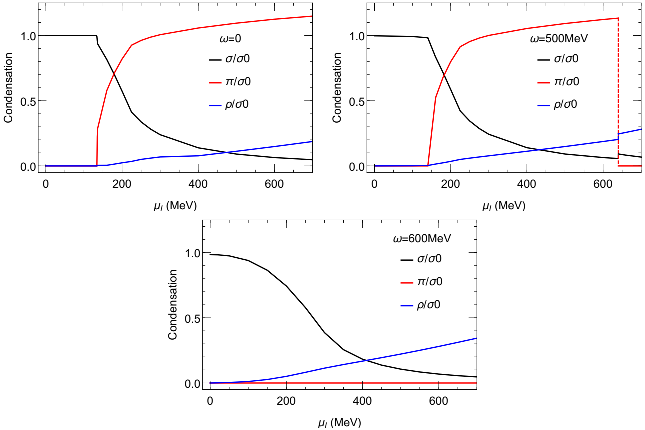

Figure: σ, π, ρ dominated phase

Phase diagram in $\omega - \mu_I$

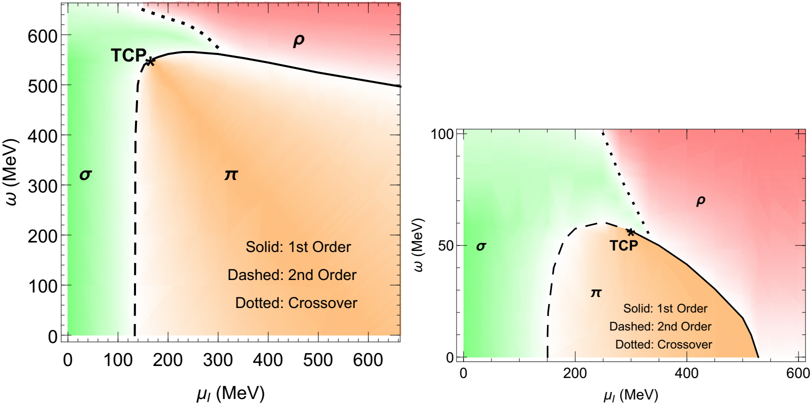

Figure: (left) $\mu = 0$, (right) $\mu = 250 MeV$

New phase diagram, New Tri-Critical End Point!

Conclusion

- pion and rho meson superfluidity under rotation in NJL model.
- inverse catalysis effect on the pion superfluidity (spin-0 channel).
- Rotation weaken spin 0 condensate (1606.03808). And enhance nonzero ones (this work).
- Rho condensate at T=mu=0 with none zero isospin chemical potential under rotation.
- A new type phase diagram in the $\omega - \mu_I$ plane and a new TCP $\sim (\mu_I^c = 165, \omega^c = 548)$ MeV.

Vorticity

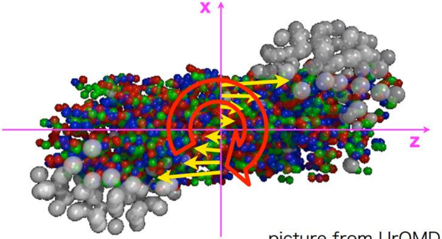

picture from UrQMD

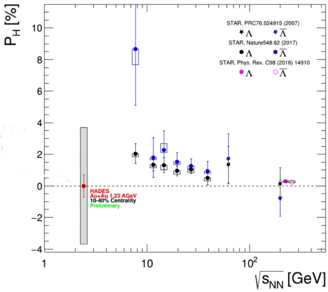

STAR, Nature 2017

- Orbital momentum $L_y = \frac{Ab\sqrt{S_{NN}}}{2} \sim 10^{4-5}\hbar$
- global kinetic vorticity $\vec{\omega} = \frac{1}{2}\nabla \times \vec{v} \sim 10^{21}s^{-1}$

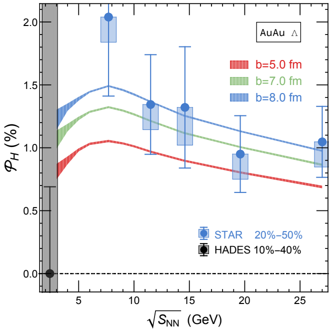

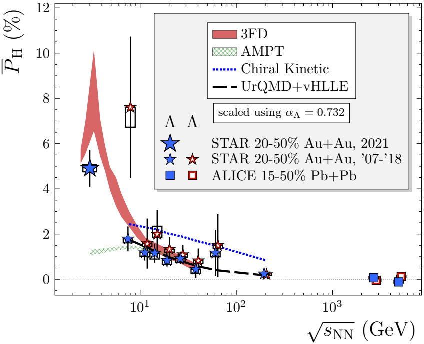

STAR, PRC104(2021)6,L061901

Many other novel phenomena

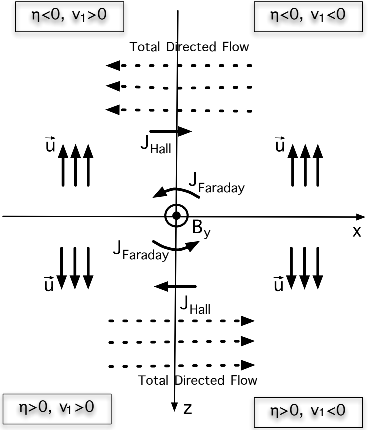

PRC89(2014)054905

Thank you for your attention!